Ceramics-Silikáty 65 (4), 344-353 (2021)
www.ceramics-silikaty.cz doi: 10.13168/cs.2021.0036

A NOVEL METHOD TO SYNTHESIS OF CALCIUM SULPHATE ANHYDRITE SELF-DOPED WITH SiO_2 FROM RED MUD AS A BIOCERAMIC

ELİF UZUN KART

Metallurgical and Materials Engineering, Marmara University, İstanbul, Turkey

#E-mail: elif.uzun@marmara.edu.tr

Submitted July 12, 2021; accepted September 15, 2021

Keywords: Calcium Sulphate Anhydrite, Self –Doped with SiO_2, Bioceramic, Red Mud

In this study, red mud was used to synthesis of calcium sulphate anhydrite (CSA) self-doped with SiO_2 for production bioceramic. The agitation sulphuric acid leaching method was used at atmospheric conditions to synthesis of CSA powder that was pressed as green body pellets for sintering procedure at a temperature varying from 800 °C to 1200 °C. After sintering, mechanical, chemical and in vitro tests were performed to determine the optimum parameters for bioceramic production. The in vitro tests were conducted to determine the biodegradability and bioactivity characteristics of sintered--CSA (S-CSA). CSA powder was synthesized at optimum leaching parameters (95 °C, 14 M H_2SO_4, 0.10 (w/v), 180 min.), its mineralogical composition was CSA (97.9 %) and SiO_2 (2.1 %). Density, compressive strength and hardness were reached 2.65 g·cm^{-3}, 114.67 MPa and 149.20 HV, respectively at 1100 °C of S-CSA pellets. As the temperature increased wollastonite/larnite phases formed. The homogenous bone-like structure hydroxyapatite phase was detected at 28th day of the in vitro test. As a conclusion, bioactive CSA self-doped with SiO_2 could be produced directly from red mud in a single step, without using additional substances and that was obtained to ensure the use as a bioceramic.

INTRODUCTION

Red mud (RM) is a waste product released during the production of alumina from bauxite ore with the Bayer Process [1, 2]. Since RM contains iron, titanium, aluminum minerals, silica, sodium aluminum hydro silicates, calcium compounds, and rare earth elements, which cannot be dissolved in sodium hydroxide solution, it can be used as a secondary raw material [1]. RM contains large amounts of Fe_2O_3, SiO_2, Al_2O_3 with secondary oxides TiO_2, CaO, and MgO suitable in the production of glass, ceramics or cements [3]. Ceramic materials are quite compatible with the biomaterials that are used to perform certain characteristics and functions in medical applications. Bioceramics are corrosion-resistant, anti-allergic and non-toxic, low-density inorganic materials, and have superior friction characteristics. When they are processed with the convenient method, they can remain in the body for a long time and do not decompose because of their chemical inactivity and as they are insoluble [4]. The use of bioceramic materials reduced the wear-and-tear rates of the components and the amount of the released ion to negligible levels [5]. These advanced ceramics are employed in orthopedic surgery, dental implants, as a bone filler, and for tissue engineering scaffolds [6]. According to the interactions of bioceramics with tissue, they are listed under three main groups as bioinert, bioactive, and biodegradable [6-19]. Most of the bioactive ceramics are based on calcium phosphate materials (hydroxyapatite; (HA)) are quite similar to the mineral aspect of the bones, but their load-bearing capacity is lower [20]. However, biodegradable ceramics are tricalcium phosphate (TCP) and calcium sulphate ($CaSO_4$; CS) are used as "bone powder" [21, 22]. Rapid degradation of this materials might cause cellular death so the degradation rates must coincide with the growth rates of new bones [23].

CS has been used since 1892 in orthopedic surgery as a bone void filling treatment that has biological advantages such as biodegradability and bioactivity [24]. It is converted into CS-dihydrate ($CaSO_4 \cdot 2H_2O$; CSD), which is considered to be one of the most successful bioceramic; however, its high dissolution rate poses an important disadvantage (it completely degrades in 4 - 7 weeks) and is much faster than the growth of new bones [25]. In this context, it is very important to increase the strength of CSs and decrease the degradation rates for using them as bioceramic. Sintering technique is applied to increase the strength of CS and decrease its degradation rates, and several grain growth inhibitors (SiO_2, P_2O_5, CaO, and $NaHCO_3$) are added. Since increased grain size causes decreased strength values, various grain growth inhibitors are often added to CS to avoid this [26-30].

Therefore, in this study, optimum conditions of atmospheric sulfuric acid agitation leaching, sintering, and in-vitro testing were investigated for the producibility of CSA self-doped with SiO_2, as a bioceramic used in medical applications, from red mud which has never been evaluated before, using chemical (X-ray diffractometer (XRD), scanning electron microscopy (SEM) and energy-dispersive X-ray spectroscopy (EDX)) and mechanical (density, hardness, compressive strength) analyses methods.

EXPERIMENTAL

Materials, Analyses, and Characterization of Samples

In the experimental studies, RM, which is the waste of a metallurgical plant in Turkey-Seydişehir produced metallic aluminum by Bayer process, was used for CSA synthesis. XRD and ICP-OES analyses for oxide composition of RM sample studied are given in Figure 1 and Table 1. RM's XRD analyses have been performed at 1,5405 Å wavelength with CuKα radiation via using Bruker D8 advance diffractometer. The main phases found are hematite, calcite, quartz, gibbsite, ilmenite minerals. XRD analyses are supported with ICP-OES analysis (Table 1). Iron (25 %) was found in the hematite structure of RM, and aluminum (10 %) was detected in gibbsite, titanium (3 %) was observed in ilmenite and perovskite, and calcium (2.7 %) was seen in calcite phases. It was confirmed that a significant amount of rare earth elements such as Sc, Sr, Y, Nb are doped in the crystal structure of hematite, silica, and cancrinite in RM, not in a free structure in the XRD pattern, and was detected in the ICP-OES elemental analysis. In this study, calcium (2.5 %) and silica (7.5 %) in RM were employed to produce CSA self-doped with SiO_2, which is a bioceramic raw material.

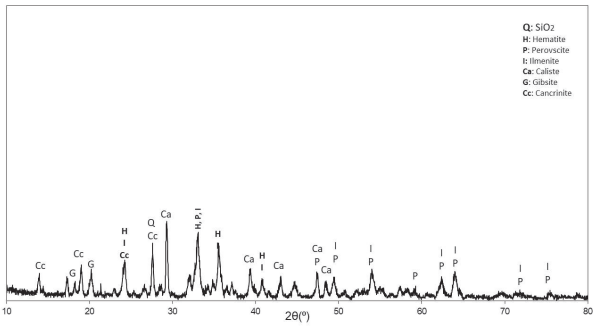

Figure 1. X-ray diffraction pattern of RM.

Table 1. Oxide composition of RM.

Oxide Composition	Amount (weight %)
Fe_2O_3	59.21
Al_2O_3	20.11
SiO_2	15.22
CaO	2.93
TiO_2	4.27
MgO	0.90

The RM has alkali media because of caustic soda usage for the Bayer process digestion step. Since it is a leaching process waste, no size reduction was applied to RM has been found that 80 % of RM's finer than 7 µm.

In experimental studies intended for the CSA synthesis process, Sigma Aldrich (MERCK) quality sulfuric acid (96 %; d:1.84 $g \cdot cm^{-3}$) and de-ionized water was used. Sulfuric acid was used to dissolve all the impurities in the RM content into the ionic phase, and to form the source of sulphate ions in leaching experiments. Simulated body fluid (SBF) was used in in-vitro experiments. SBF was prepared according to the procedure that was described by Kokubo et al., 2003 with Sigma Aldrich (MERCK) quality NaCl, $NaHCO_3$, HCl, $K_2HPO_4 \cdot 3H_2O$, $MgCl_2 \cdot 6H_2O$, HCl, $CaCl_2$, Na_2SO_4, tris(hydroxymethyl) aminomethane chemicals [31]. In the formation of the CSA pellets, a hydraulic press (Compac Brand) that had a 1000 MPa pressure capacity and a mold that was made of duplex steel, hardened by heat treatment, designed by ourselves, were used. Microhardness device (Shimadzu Brand) was used for the mechanical tests of CSA/S-CSA pellets, and a compression device (Devotrans Brand) was used to calculate the compressive strength, and the archimedean system was used for density calculations.

Synthesis Process of CSA

The agitation sulfuric acid leaching technique was used at atmospheric conditions in the synthesis experiments. The physical water of RM was removed at 105 °C for 24 hours and dried RM was stored in vacuum containers was used in leaching experiments. Synthesis experiments were performed in a water bath experimental procedure given in Figure 2. An external rotor was placed into the reactor to provide agitation, and a thermocouple in a water bath to keep the temperature constant. The temperature of the leaching solution was kept under control by using a thermocouple that had ± 5 °C accuracy throughout the experiments.

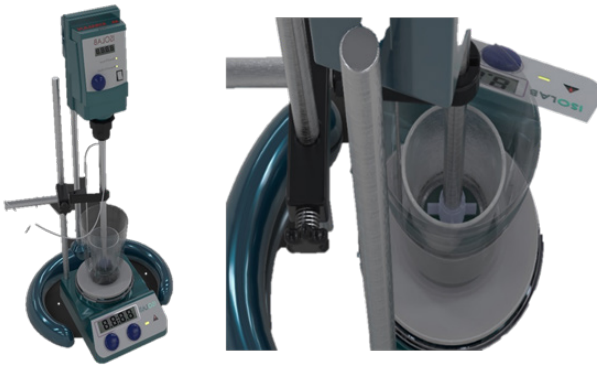

Figure 2. Experimental procedure of CSA synthesis.

The agitation speed was kept constant at 160 rpm to suspend the RM particles and to avoid adhesion to the reactor wall with the effect of centrifugal force. All other leaching parameters (i.e. leaching time, leaching temperature, solid/liquid ratio, and acid concentration) were planned as the conditions in which all the impurities except for Ca and Si in RM were dissoluted to the solution. As a result of the experiments, leaching temperature was determined to be 95 °C, acid concentration 14 M H_2SO_4, solid/liquid ratio 0.10 g·ml^{-1}, and leaching time 3 h. Once the synthesis process was completed, vacuum filtration, repeated washing with de-ionized water, and drying at 65 °C for 24 hours were followed to obtain CSA in the solid phase. The CSA, which was removed from its physical water, was characterized with XRD, SEM, EDX analyses. As a result of the synthesis studies, 10.0001 g moisture-free RM was leached and as a result 4.1020 g dry CSA self-doped with SiO_2 was produced.

Preparation and Sintering Process of CSA Pellets

CSA powder was pressed into pellets 5 mm in diameter and 6mm in thickness at a uniaxial pressure of 350 MPa which are named green body CSA pellets (Figure 3a, b). The powders that stick to the mold wall during pressing cannot transmit the applied load to the other powders, close to them homogeneously, and cause the production of pellets with heterogeneous pressure, and based on this, heterogeneous density [32]. The mold walls are coated with a mixture of 2 % of zinc stearate and ethyl alcohol according to weight before each pelleting process to minimize this situation, ensure a better sliding of the powders on each other, and reduce the wear-and-tear of the mold walls. The resulting CSA pellets are in green body form, which cannot remain stable as in the given form, and can become powder again (Figure 3b). The CSA pellets were sintered at a temperature varying from 800 °C to 1200 °C in atmospheric conditions for 1 h, with heating and cooling rates of 5 °C·min^{-1}. For the characterization of the S-CSA pellets resulting with sintering, mechanical, phase transformation, chemical composition, and microstructure characteristics were determined with compression, hardness, density, XRD, SEM, and EDX analyses. SEM was used for investigation of the microstructure of S-CSAs. The S-CSAs elemental composition were analysed with EDX, and XRD was utilized to characterize the phase transformation of S-CSAs at 800 °C to 1200 °C temperatures. All the processes and products until the S-CSA production phase flowsheet is given in Figure 4.

a) b)

Figure 3. CSA a) powder, b) green body.

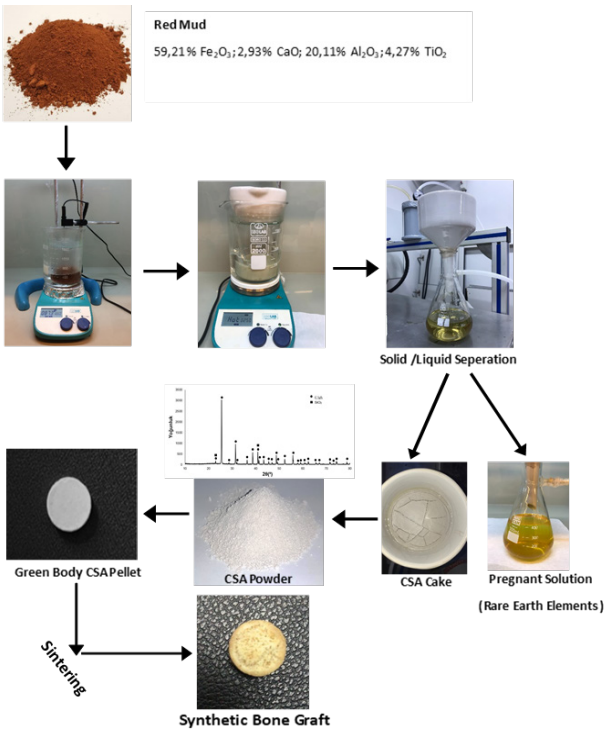

Figure 4. Experimental flowsheet of the whole procedure.

In Vitro Test Process in SBF

In vitro tests were performed to determine the optimum sintering temperature for bioceramic production according to the biodegradability, and bioactivity characteristics of the sintered green body CSA pellets at all temperatures. Simulated body fluid was used in the tests. SBF is a cellular, protein-free, saturated phospho-calcium solution with ionic composition nearly the same as human blood plasma. Kokubo et al. (2003) described the preparation of SBF. It is important when preparing the SBF that the chemicals do not settle, there is a visible, colorless and transparent solution, the temperature is 36.5 °C, which is the body temperature, and the solution is made in a polypropylene beaker. After a careful pH adjustment to 7.40, the beaker is filled up to 1 liter. And the fresh SBF solution is preserved at 5 °C for up to 30 days. Biological tests were started after the solution was prepared, and the pellets were passed to fresh SBF every 24 hours at a rate of 10 ml SBF for each 1 g of S-CSA, and the biodegradability, and bioactivity characteristics were investigated within 28 days.

The renewal of the SBF every 24 hours was determined for the simulation of the in vitro medium to the in vivo medium, and the continuation of the tests throughout 28 days was determined because the bone formation was completed within at least 28 days in the human body [33].

RESULTS AND DISCUSSION

Characterization of CSA/S-CSA

CSA

After the atmospheric agitation acid leaching applied to the RM sample at optimum parameters (95 °C, 14 M H_2SO_4, 0.10 (w/v), 180 min.), it was determined that all of the peaks in the XRD pattern of the leached solid waste (insoluble solid after leaching) consisted of CSA (97.9 %) and SiO_2 (2.1 %) (Figure 5). The fact that this main phase, which was synthesized, was CSA, which has been used as a bioceramic and that the other phase was SiO_2 emphasized that it can be made use of as a CSA self-doped with SiO_2 [24].

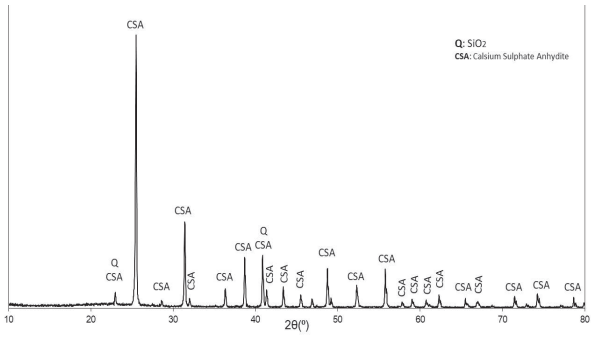

Figure 5. Synthesized CSA XRD pattern.

The XRD peaks observed at 2Θ values 23.04 and 40.90 in Figure 5 indicated that the SiO_2 and both of the other peaks observed only CSA as the main component. The CSA formation equations of RM, which were preferred as a source of calcium and silica, with the H_2SO_4 leaching, are given below (Equations 1-3) [34, 35];

$$CaO + H_2SO_4 \rightarrow CaSO_4 + H_2O \quad (1)$$

$$CaCO_3 + H_2SO_4 \rightarrow CaSO_4 + H_2O + CO_2 \quad (2)$$

$$CaTiO_3 + 2H_2SO_4 \rightarrow CaSO_4 + TiOSO_4 + 2H_2O \quad (3)$$

According to its amount of crystallized water, CS exists in 3 different chemical forms as anhydride, hemihydrate, and dehydrate [35]. Although CS-Hemihydrate (CSH) has been used as a bone void filler in medical applications, its negative aspects, such as rapid degradation and low strength have led to the search for slowly-degrading biomaterials in body fluid [29, 36]. Studies showed that the degradation rate of CSA is slower than CSH [30, 37]. When the limitations of the use of CSH were considered in this study, CSA, which is believed to have a high potential for being used as a bone void filler, was synthesized after the leaching process from RM, which is the subject of many studies, released in very high amounts and cannot be put into practice for recycling. The comparative XRD pattern of the RM and synthesized CSA from RM by atmospheric sulfuric acid leaching is given in Figure 6.

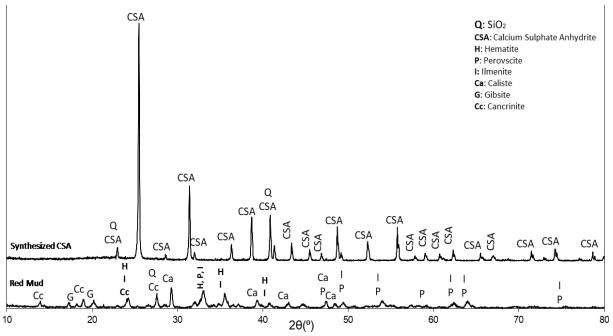

Figure 6. XRD patterns of the red mud and synthesized CSA after leaching at indicated conditions.

The XRD peaks observed at 2Θ values 29.28, 39.44, 43.16, 47.48 and at 2Θ values 17.38, 20.2 in Figure 6 indicated that the calcite and gibbsite, respectively. In addition, Figure 6 showed that the red mud contained quartz, cancrinite, ilmenite, perovskite, and hematite as the other main components. Also, Figure 6 show that all the structures in the RM decomposed, the metals were dissolved, and the sulphate ions in the sulfuric acid made compounds with calcium to form CSA, and the quartz remained as a self-doped material.

S-CSA

The surface area of the powders increases with sintering, and the area of the grain boundaries decreases [38]. However, since the increased grain size causes decreased strength values, various grain growth inhibitors are often added to avoid this. These inhibitors also prevent growth by settling in grain boundaries [28]. In their study, Kuo et al. (2013) increased the density and strength of CS with additives such as SiO_2, P_2O_5, CaO, and $NaHCO_3$. They also demonstrated the adjustability of the degradation rates by sintering with the correct additive [30]. Chang et al. (2015) added bioactive glass at a rate of 1 % by weight into CS powder. Glass-added CS pellets were subjected to sintering at 900 °C for 1 hour, and although the glass amount was low, the compressive strength of the pellets increased by 40 % and the degradation rate decreased [28]. Chang et al. (2017) found that adding SiO_2 at a rate of 1 % by weight to CS prevented the growth of CS grains during sintering and that the wollastonite phase ($CaSiO_3$) formed by the addition of SiO_2 precipitated at the grain boundaries, improved the microstructure, and

exhibited higher compressive strength [29]. Borhan et al. (2010) increased the strength values of 60 % CS and 40 % apatite (nanostructure apatite) mixture (by weight) with colloidal silica suspension (20 % by weight) [25]. Although the compressive strength was 21 MPa for pure CS, the strength value of the CS-apatite mixture decreased to 7 MPa after adding apatite. When nano-silica (20 %) was added, it increased to 19 MPa. In vivo studies conducted on CS pellets in the literature indicate that the degradation rates are very fast, and it was determined that this affects bone regeneration negatively [24, 39]. Also, the rapid absorption of CS and the rapid increase in Ca^{+2} ions may cause cellular death in the body or inflammation in the bone tissues [23]. It is already known that as a result of the rapid degradation of CS pellets, the powders settle in the body, and do not provide support for newly-formed bones. For this reason, in the present study, the synthesized CSA green body pellets were sintered at 800 °C, 900 °C, 1000 °C, 1100 °C, and 1200 °C for 1 hour under atmospheric conditions to eliminate the factors that affected the biodegradation behaviors (i.e. fast dissolution and precipitation, low strength, etc.). Factors such as chemical content, amount of micro/macro pores, powder size, and amount of crystal water affect the biological behaviors of CS. It was also reported in previous studies that the rapid degradation problem of CS can be avoided with the sintering technique, as explained in the literature [26].

The CS that was synthesized in this study was in the anhydride phase (CSA) and had self-addition SiO_2. The phase transformation of the sintering process was performed to improve the physical characteristics (i.e. hardness, compressive strength, and density), and to make the silica to be doped into the CSA crystal structure. The XRD patterns of S-CSA pellets obtained at different temperatures are given in Figure 7.

The peaks observed after sintering at 800 °C correspond well to the raw CSA peaks as intensity/2Θ values, which shows that there is no phase transformation or novel phase formation at 800 °C, and all phases are

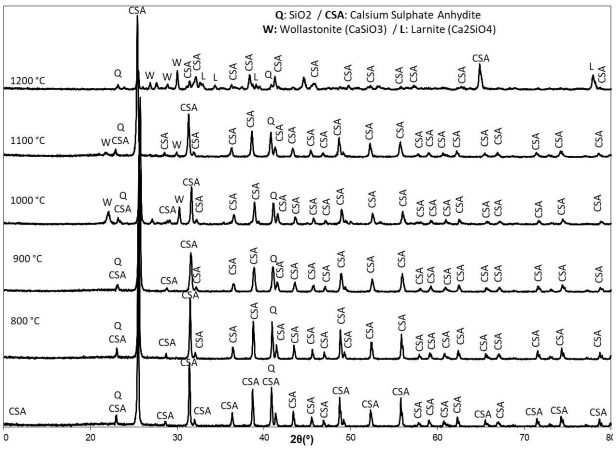

Figure 7. XRD patterns of the CSA and S-CSA pellets at indicated temperatures.

the same as in raw CSA. When the sintering temperature was increased to 900 °C, no phase changes or new phase formations were observed; however, decreased phase intensities were observed, which emphasizes that the phase change or formation will occur with increased temperature, and the presence of the same phases (CSA, SiO_2) draws attention in this respect [26]. The wollastonite ($CaSiO_3$) peaks were observed 2Θ values at 22.14 and 30.20 after sintering at 1000 °C. A slight shift in the peaks (especially at 1000 °C and 1100 °C) to the left means that the SiO_2 in the CSA obtained with the leaching process is dissolved in the CSA at high temperatures [29]. As the sintering temperature increased up to 1100 °C, the intensity of the 2Θ value of $CaSiO_3$ peaks at 22.14 and 30.20 decreased. The wollastonite peak with 2Θ value of 22.14 disappeared at 1200 °C, which was the final temperature of the sintering process. New wollastonite peaks (2Θ: 26.94, 27.6), and a new-phase larnite (Ca_2SiO_4) were formed (2Θ: 33.55, 36.46, 39.42 and 78.04). With increased sintering temperature, the degradation of CSA, formation of SO_2 gas, dissolution of SiO_2 in its body, and the formation of wollastonite and larnite are given below (Equations 4-8) [40].

$$2CaSO_4 \rightarrow 2CaO + 2SO_2 + O_2 \quad (4)$$

$$2CaO + SiO_2 \rightarrow Ca_2SiO_4 \quad (5)$$

$$CaO + SiO_2 \rightarrow CaSiO_3 \quad (6)$$

$$Ca_2SiO_4 + SiO_2 \rightarrow 2CaSiO_3 \quad (7)$$

$$6CaSO_4 + 4SiO_2 \rightarrow 2CaSiO_3 + 2Ca_2SiO_4 + 6SO_2 + 3O_2 \quad (8)$$

Micro-cracks and porosities are formed between the grains when the sulfur in the structure leaves the material at high temperatures (by passing into the SO_2 gas phase) [40]. It was observed that the pellet form deteriorated and fragmented in S-CSAs obtained as a result of the experiments in which the sintering temperature was increased up to 1200 °C. It can be observed that the deterioration in the form of the pellets at 1200 °C occurred because of the decomposition of the sulfur in the CSA structure as SO_2 gas. For this reason, since S-CSA was not in pellet format, its physical characteristics could not be identified, and the temperature of 1200 °C was excluded from the optimum parameters. The mechanical characteristics of S-CSA pellets are given in Figure 8a, b, c. It is seen in this figure that the density values increase depending on the increased sintering temperature (Figure 8a) [29]. The hardness values of the pellets that were sintered at 800 - 1100 °C for 1 hour are given in Figure 8b. Although the pellets that were sintered at 800 °C had the lowest density value as 2.09 $g \cdot cm^{-3}$, it increased to 2.16 $g \cdot cm^{-3}$ with an increased temperature of 900 °C. A sudden increase was detected in the density value (2.55 $g \cdot cm^{-3}$) at 1000 °C, and it was measured as 2.65 $g \cdot cm^{-3}$ at 1100 °C (Figure 8a). Also, it can be observed that the increased density values at 1100 °C are related

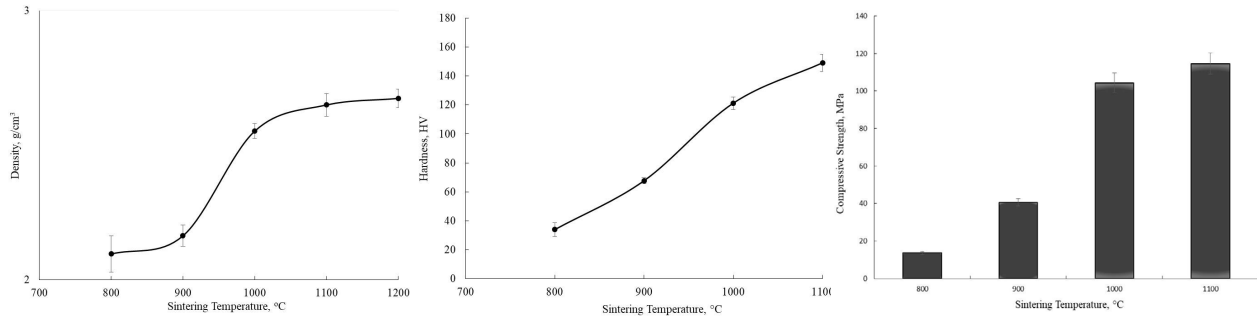

a) b) c)

Figure 8. Density (a), hardness (b), and compressive strength (c) of S-CSA pellets at indicated sintering temperatures.

to the formation of $CaSiO_3$ [29]. The surface area of the powders increases and the area of the grain boundaries decreases with sintering [38]. As reported in the literature, the hardness and compressive strength values increased in direct proportionally to the density value as the temperature increased with SiO_2 in synthesized CSA structure (Figure 8b, c). As the temperature increased, the hardness values were measured as 33.90 HV, 67.68 HV, 121.32 HV, and 149.20 HV, respectively (Figure 8b). Compressive strength values reached 13.67 MPa at 800 °C, 40.67 MPa at 900 °C, 104.33 MPA at 1000 °C, and 114.67 MPa at 1100 °C (Figure 8c). The strength of ceramic is controlled by its microstructure, such as density and grain size. The presence of silica can further enhance the strength through microstructure refinement. Also, compressive strength can be associated with the formation of the wollastonite ($CaSiO_3$) phase occurring with increased temperature [29]. The formation of $CaSiO_3$ particles prohibits the diffusion between $CaSO_4$ grains, the S-CSA density is increased because of this. As seen in the SEM images, the grains did not grow as the temperature increased, but the pores increased in a way that the density, hardness, and strength values were at their highest levels (Figure 9). As the temperature increased, the shrinkage of the grains occurred as a result of the SiO_2 dissolving in the structure of the synthesized CSA acting as an inhibitor. It is seen in the SEM images taken after sintering in Figure 9 that the grain sizes decreased as the sintering temperature increased. It was confirmed that the improvement of the microstructure and the increased strength were because of the effect of $CaSiO_3$ formed by the dissolution of SiO_2. It was observed that the porosities increased at 1100°C when grain sizes decreased (Figure 9d), which was supported by the images in which the sulfur in the CSA was removed as SO_2 gas, forming gaps at the same time.

Bioactivity Characterization of S-CSA

For bioactivity tests, S-CSA pellets that were obtained at all temperatures were incubated in a simulated body fluid (i.e. physiological solution) by taking fresh SBF into them every 24 hours for 28 days. The images of the CSA pellet (at the time of contact with body fluid) and S-CSA pellets (at the end of the 28th day) taken at the end of the SBF testing are given in Figure 10. As seen in the images, the pellet formation quickly degraded when CSA green body came into contact with SBF. Unlike

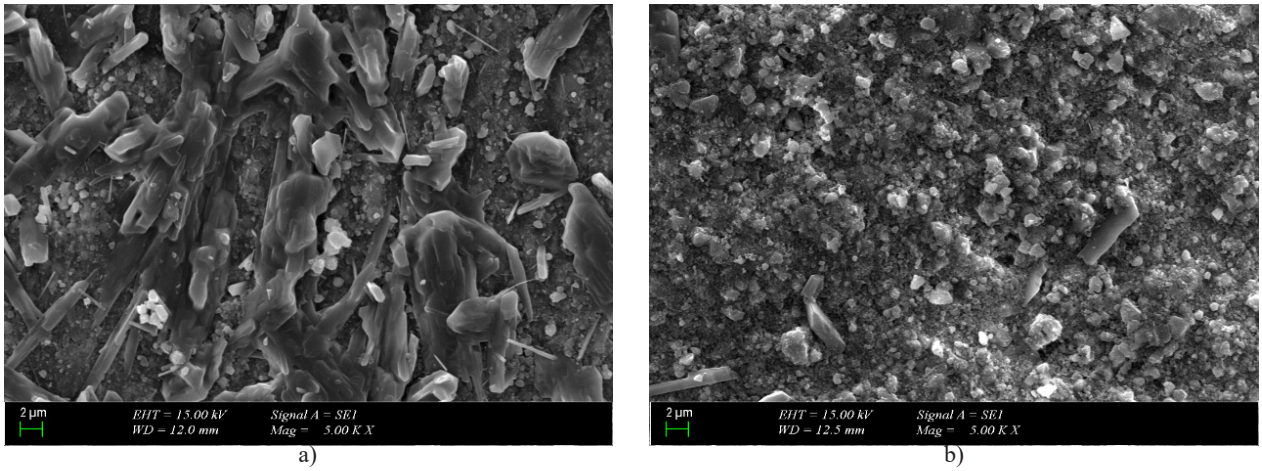

a) b)

Figure 9. SEM images of S-CSA after sintering at a) 800 °C, b) 900 °C, c) 1000 °C and d) 1100 °C. *continue on the next page...*

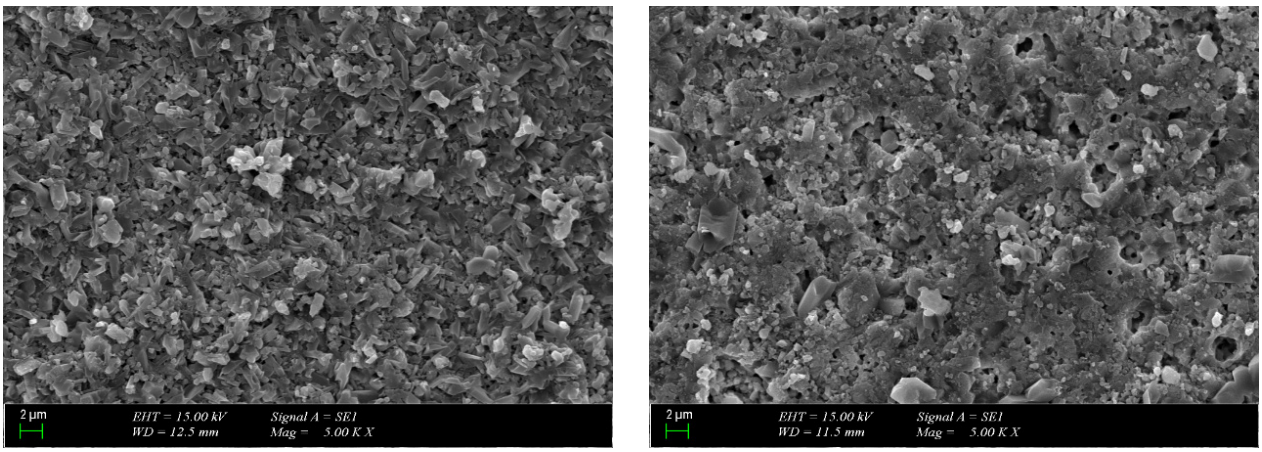

c) d)

Figure 9. SEM images of S-CSA after sintering at a) 800 °C, b) 900 °C, c) 1000 °C and d) 1100 °C.

the literature data, although calcium sulphate is in the anhydrite phase, its disintegration when it comes into contact with SBF shows that the presence of the CSA phase is not enough alone for it to be used as a bioceramic, and sintering is required. As shown in Figure 10b, S-CSA pellets did not degrade in SBF for 28 days at the lowest sintering temperature of 800 °C. Similarly, no changes were detected in the pellet form for 28 days in S-CSA pellets at all other temperatures. Contrary to the literature data, it was observed that even S-CSA pellets that were obtained at temperatures of 800 °C and 900 °C were bioactive. Although additives (SiO_2) were added to CSA obtained with traditional methods, when it was sintered below 1100 °C, degradation was seen in in-vitro tests [27-30]. However, in this study, the S-CSA self-doped with SiO_2 pellets that were obtained by sintering CSA that was synthesized from RM at low temperatures did not degrade in SBF for 28 days.

The XRD patterns of the pellets that reacted with Na^+, K^+, HPO_4^{2-}, HCO^-, Cl^-, Ca^{2+}, Mg^{2+}, SO_4^{2-} ions in the SBF were obtained at the end of the 28th day (Figure 11). The forms of S-CSA pellets that were sintered at 800 °C did not change, and there was no change in their patterns before and after the testing. The HA (at 2Θ; 44.9, 64.7, 78.16) and wollastonite (W) (at 2Θ; 30.24, 41.60, 43.68) peaks, which were not detected before the testing, were detected in the post-test degradation patterns of S-CSA pellets that were sintered at 900 °C. It was also detected that the number of HA and W peaks increased with increased sintering temperature, the CSA peaks were replaced by HA peaks, and novel HA and W peaks formed. The HA that formed at the end of the 28th day showed that the resulting pellets were bioactive. It also showed that it gained bioactivity since it did not decompose [27, 29, 38, 40]. CSA peaks and newly formed HA peaks were observed at 2Θ values 22.58, 31.48, 52.5, 56.06 of S-CSA at 1000 °C - 1100 °C. Although no wollastonite peaks were detected before the in vitro test in the XRD patterns of S-CSA pellets obtained at 900 °C, they were observed at 22.12Θ, 27.08Θ, and 50.22Θ levels at the end of the SBF test, which shows that the CSAs coated on the surfaces of the pellets dissolve (by releasing Ca^{2+}), and the $CaSiO_3$ structures that exist in the surface.

It was observed on the surface of the S-CSA pellet, which was sintered at 800 °C, and which consisted of bar-like grains before the in vitro testing, that the bar-like grains were replaced by granular grains after the

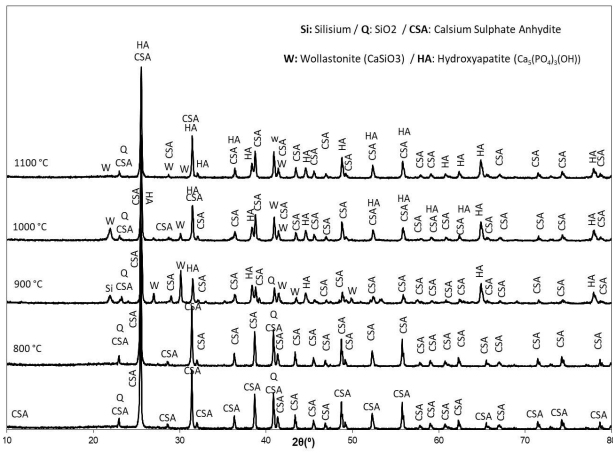

Figure 11. XRD patterns of S-CSA pellets after in vitro SBF tests during 28 days.

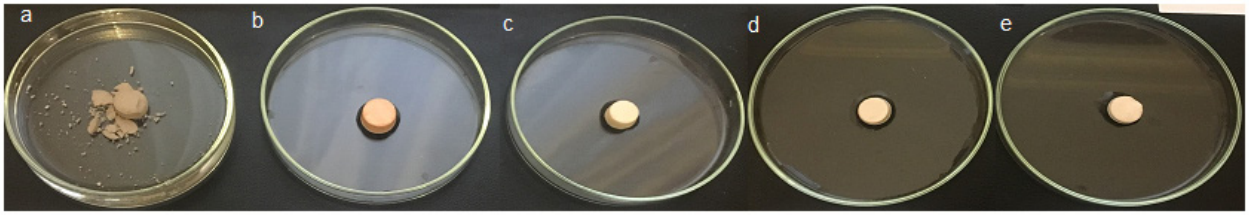

Figure 10. The pellets with completed bioactivity tests in SBF a) CSA, b) 800 °C, c) 900 °C, d) 1000 °C, e) 1100 °C S-CSA.

in vitro testing, and pores were formed in many places (Figure 12). It was also observed that bar-like connections formed between the granular and porous structures. As mentioned in the literature, it can be reported that the porosities are caused by the removal of the Ca^{2+} ions that are released from CSAs. S-CSA pellets, which were sintered at 900 °C before in vitro testing, particle size decreased when compared to at 800 °C, and their bar-like structures disappeared (Figure 9b). After in vitro testing, glassy-melted areas appeared on the surface, and homogeneous bone-like structures began to form. When compared with XRD patterns, melting structures that supported the formation of W peaks after in vitro testing, which were not detected in in-vitro testing, and it was also supported that HA structures appeared with homogeneous bone-like structure appearance. When the temperature was elevated up to 1000 °C, it was seen that the homogeneous bone-like structure seen at 900 °C completely covered the pellet surfaces, the melting or porous structures disappeared completely, and the whole surface was covered with HA. Although rarely, accumulated pure calcium flakes were detected only at 1000 °C because of the excess Ca^{2+} ions. When the S-CSA pellet that was sintered at 1100 °C, it was seen that the molten structures were distributed to the surface completely, and the HA structures and pure calcium flakes almost disappeared. In this image, it was proven that the wollastonite structures increased as the temperature increased. The bioactivity is reported as function of wollastonite presence and its content. It can be observed with the SEM of samples sintered at 1000 °C, where wollastonite was the most detected. Sintered at 1100 °C, larnite formation occurred and the HA formation was decreased.

CONCLUSION

The synthesis of CSA powder that contained SiO_2 from RM, which is a Bayer Process waste, into S-CSA self-doped with SiO_2 form, and obtaining bioceramic by determining optimum conditions were investigated in this study. The synthesis of CSA powder by atmospheric sulfuric acid agitation leaching under the optimum conditions (H_2SO_4 concentration: 14 M; leaching time: 180 min; temperature: 95 °C; solid/liquid ratio: 0.10 $g \cdot ml^{-1}$). XRD patterns was analysed for the synthesized CSA powder, and it was found that all peaks were 97.9 % CSA, 2.1 % SiO_2. Considering that 100 000 tons of RM is sent to the tailings dam every year when calculated as industrial production, 1 000 tons of CSA can be synthesized annually from Turkish RM. Sintering of CSA powder to produce S-CSA self-doped with SiO_2 pellets at 800 °C, 900 °C, 1000 °C, 1100 °C, and 1200 °C temperatures. The density, hardness, and compressive strength characteristics of S-CSA pellets were identified to determine the optimum sintering temperature. Since the pellets that were sintered at 1200 °C lost most of their sulfur as SO_2, they were disintegrated during the sintering step and were excluded from the scope of the testing. As the temperature increased, the density, hardness, and compressive strength values also increased to 2.65 $g \cdot cm^{-3}$, 149.20 HV, and 114.67 MPa, respectively, for the S-CSA pellets obtained at 1100 °C. In the XRD patterns, CSA was detected at all temperatures as of 900 °C, wollastonite aside from SiO_2, and larnite phases at 1200 °C. The S-CSA pellets obtained at temperatures of 800 °C (no wollastonite phase was formed), and 1200 °C (since it decomposed during sintering) were excluded from the bioceramic production conditions. In vitro tests were done for optimization of bioactivity, and biodegradability characteristics. After in vitro tests HA formation was detected in all S-CSA pellets that were sintered after 900 °C. It was found that all the surfaces of the pellets were covered with HAs of the same bone-like structure at 1000 °C with a perfect bioactive surface was obtained because of the wollastonite phase remained below the HA precipitates.

As a conclusion, unlike the classical methods, a CSA that contained self-doped with SiO_2 could be produced directly from red mud in a single step, without using additional substances, and bioactive CSA self-doped with SiO_2 that is suitable for in vitro conditions was obtained to ensure the use as a bioceramic.

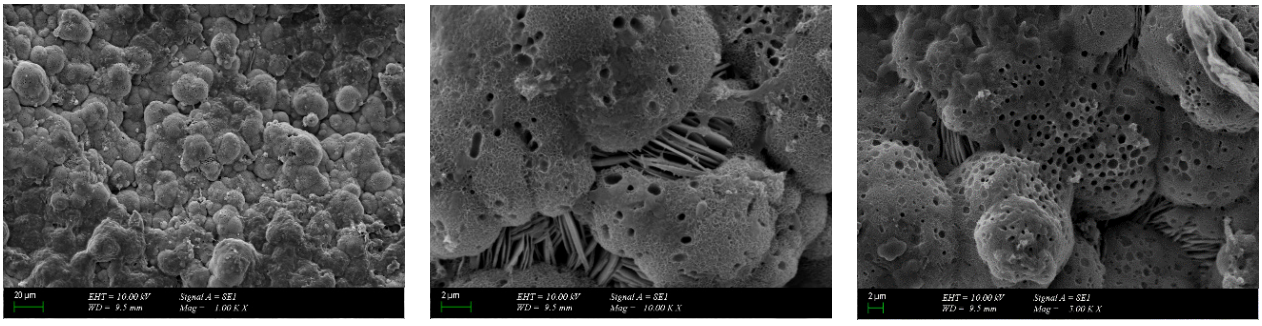

a) b) c)

Figure 12. SEM images of the S-CSA pellets subjected to in vitro tests.

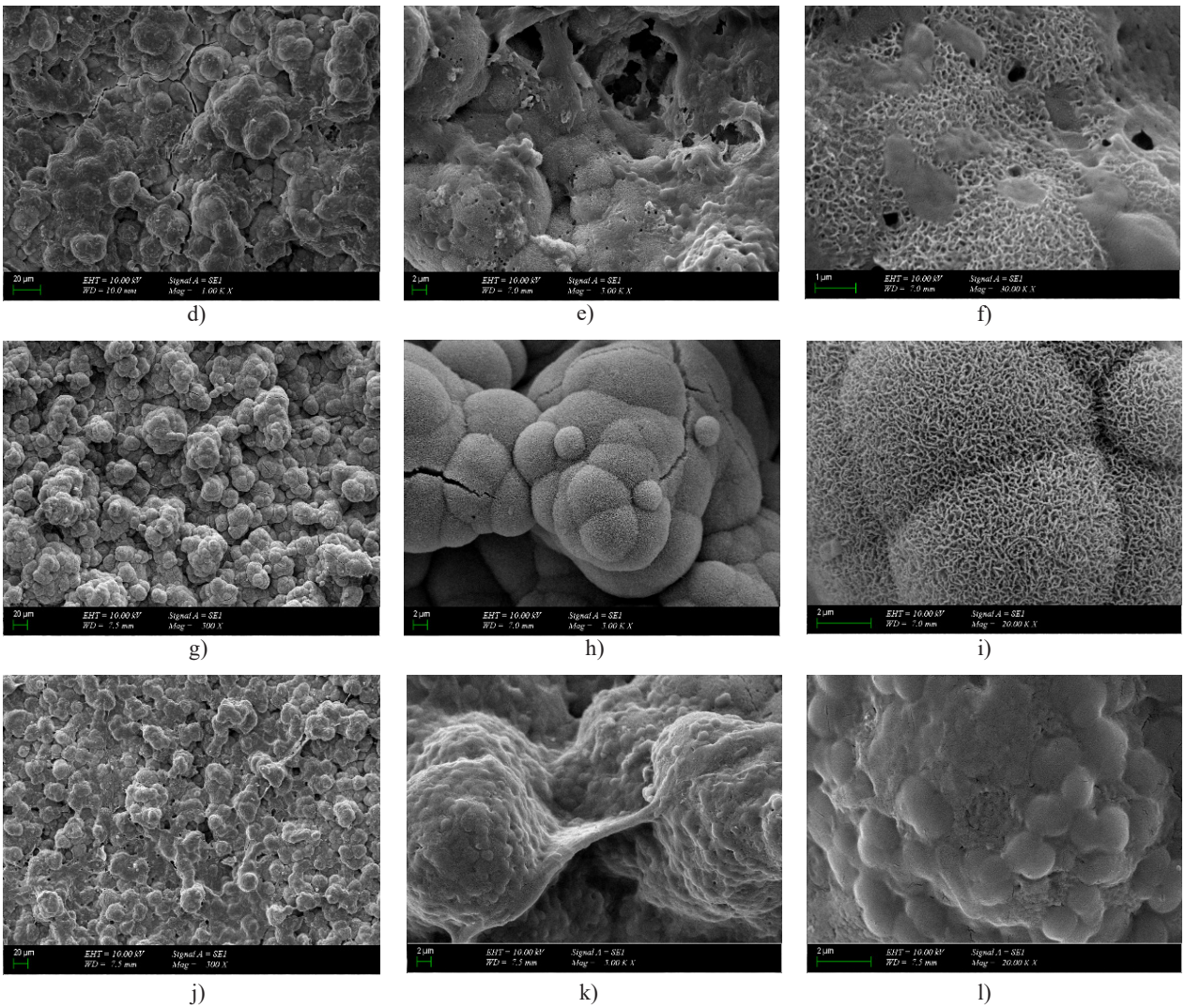

Figure 12. SEM images of the S-CSA pellets subjected to in vitro tests.

Acknowledgment

The supply of RM samples by Eti Aluminyum A.Ş. is thankfully acknowledged.

REFERENCES

1. Anawati J., Azimi G. (2019): Recovery of scandium from Canadian bauxite residue utilizing acid baking followed by water leaching. *Waste Management*, *95*, 549–559. doi: 10.1016/j.wasman.2019.06.044
2. Rivera R.M., Ulenaers B., Ounoughene G., Binnemans K., Gerven T.V. (2018): Extraction of rare earths from bauxite residue (red mud) by dry digestion followed by water leaching. *Minerals Engineering*, *119*, 82–92. doi: 10.1016/j.mineng.2018.01.023
3. Hench L.L., Jones J.R. (2005). *Biomaterials,artificial organs and tissue engineering*. Cambridge England: Woodhead Publishing Ltd.
4. Wataha J.C. (2001): Principles of biocompatibility for dental practitioners. *Journal of Prosthetic Dentistry*, *86*(2), 203-9. doi: 10.1067/mpr.2001.117056
5. Bauer T.W., Muschler G.F. (2000): Bone graft materials. An overview of the basic science. *Clinical Orthopaedics and Related Research*, *371*, 10-27.
6. Bulut M., Karakurt L. (2011): Seramikler. *TOTBİD Dergisi*, *10*(2), 87-95.
7. Hench L.L. (1998): Bioceramics. *Journal of the American Ceramic Society*, *81*, 1705-1728. doi: 10.1111/j.1151-2916.1998.tb02540.x
8. Durmuş A.S. (2015): Kemik Grefti Yerine Doğal Bir Biyoseramik: Deniz Mercanı. *Fırat Üniversitesi Sağlık Bilimleri Veteriner Dergisi*, *29* (2), 145-150.
9. Moore W.R., Graves S.E., Bain G.I. (2001): Synthetıc Bone Graft Substıtutes. *ANZ Journal of Surgery*, *71*, 354–361. doi: 10.1046/j.1440-1622.2001.02128.x
10. Campana V., Mılano G., Pagano E., Barba M., Cıcıone C., Salonna G. , Lattanz, W., logroscino G. (2014): Bone substitutes in orthopaedic surgery: from basic science to clinical practice. *Journal of Materials Science: Materials in Medicine*, *25*(10), 2445-61. doi:10.1007/s10856-014-5240-2
11. Bhat S.V. (2002). *Biomaterials*. 1st ed., Pangbourne, England: Alpha Science International Ltd.
12. Bohner M. (2010): Resorbable biomaterials as bone graft substitutes. *Materials Today*, *13*(1-2), 24–30. doi:10.1016/

s1369-7021(10)70014-6.
13. Greenwald A.S., Boden S.D., Goldberg V.M., Khan Y., Laurencin C.T., Rosier R.N. (2001): American Academy of Orthopaedic Surgeons. The Committee on Biological Implants. Bone-graft substitutes: facts, fictions, and applications. *JBJS*, *83*(2), S98-103. doi: 10.2106/00004623-200100022-00007.
14. Uchida A., Nade SM., Mccartney E.R., Chıng W. (1984): The use of ceramics for bone replacement. A comparative study of three different porous ceramics. *The Journal of Bone and Joınt Surgery*, *66*(2), 269-275. doi: 10.1302/0301-620X.66B2.6323483
15. Şimşek A., Çakmak G., Cila E. (2004): Kemik Greftleri ve Kemik Greftlerinin Yerini Tutabilecek Maddeler. *TOTBİD Dergisi*, *3*, 79-91.
16. Costantino P.D., Hiltzik D., Govindaraj S., Moche J. (2002): *Bone healing and bone substitutes. Facial Plast Surg.*, *18*(1),13-26. doi: 10.1055/s-2002-19823
17. Boden S.D., Schimandle J.H. (1995): *Biologic enhancement of spinal fusion." Spine, 20*(24 Suppl), 113S-123S.
18. Chevalier J., Gremillard L. (2009): Ceramics for medical applications: A picture for the next 20 years. *Journal of the European Ceramic Society*, *29*(7), 1245-1255, doi:10.1016/j.jeurceramsoc.2008.08.025
19. Schepers E., de Clercq M., Ducheyne P., Kempeneers R. (1991): Bioactive glass particulate material as a filler for bone lesions. *Journal of oral rehabilitation, 18*, 439-52. doi:10.1111/j.1365-2842.1991.tb01689.x
20. Nilson F., Moniruzzaman S., Gustavsson J., Andersson R. (2013): Trends in hip fracture incidence rates among the elderly in Sweden 1987–2009. *Journal of Public Health, 35*(1), 125–131, doi:10.1093/pubmed/fds053
21. Prakasam M., Locs J., Salma-Ancane K., Loca D., Largeteau A., ve Berzina-Cimdina L. (2017): Biodegradable Materials and Metallic Implants—A Review. *Journal of Functional Biomaterials, 8*, 44.doi: 10.3390/jfb8040044
22. Winn S.R., Hollinger J.O. (2000): An osteogenic cell culture system to evaluate the cytocompatibility of osteoset, a calcium sulphate bone void filler. *Biomaterials, 21*(23), 2413-2425.doi: 10.1016/S0142-9612(00)00109-5
23. Adams C. S., Mansfield K., Perlot R. L., ve Shapiro I. M. (2001). Matrix Regulation of Skeletal Cell Apoptosis. *Journal of Biological Chemistry, 276*(23), 20316–20322. doi:10.1074/jbc.m006492200
24. Damien C.J., Parsons J.R. (1991): Bone Graft And Bone Graft Substitutes: A Review Of Current Technology And Applications. *Journal of Applied Biomaterials, 2*, 187–208. Doi: 10.1002/jab.770020307
25. Borhan S., Hesaraki S., Ahmadzadeh-Asl S. (2010): Evaluation of colloidal silica suspension as efficient additive for improving physicochemical and in vitro biological properties of calcium sulphate-based nanocomposite bone cement. *Journal of Materials Science: Materials in Medicine, 21*(12), 3171–3181. doi:10.1007/s10856-010-4168-4
26. Hsu P.Y., Chang M.P., Tuan W.H., Lai P.L. (2018): Effect of physical and chemical characteristics on the washout resistance of calcium sulphate pellets. *Ceramics International, 44*, 8934-8939.doi: 10.1016/j.ceramint.2018.02.088
27. Hsu P.Y. Kuo H.C., Syu M.L., Tuan W.H., Lai P.L. (2020): A head-to-head comparison of the degradation rate of resorbable bioceramics. *Materials Science & Engineering C, 106*, 110175. Doi:10.1016/j.msec.2019.110175
28. Chang M. P., Tsung Y. C., Hsu H. C., Tuan W. H., Lai P. L. (2015): Addition of a small amount of glass to improve the degradation behavior of calcium sulphate bioceramic. *Ceramics International, 41*, 1155–1162.doi: 10.1016/j.ceramint.2014.09.043
29. Chang MP., Hsu HC., Tuan WH. (2017): A Feasibility Study Regarding the Potential Use of Silica-Doped Calcium Sulphate Anhydrite as a Bone Void Filler. *Journal of Medical and Biological Engineering, 37*, 879–886 doi:10.1007/s40846-017-0253-1
30. Kuo S.T., Wu H.W., Tuan W.H. (2013): Resorbable calcium sulphates with tunable degradation rate. *Journal of Asian Ceramic Societies, 1*, 102–107.doi: 10.1016/j.jascer.2013.03.007
31. Kokubo T, Takadama H. (2006): How useful is SBF in predicting in vivo bone bioactivity? *Biomaterials, 27*, 2907–2915.doi: 10.1016/j.biomaterials.2006.01.017
32. Zyman Z.Z., Rokhmistrov D.V., Glushko V.I. (2010): Structural and compositional features of amorphous calcium phosphate at the early stage of precipitation. *Journal of Materials Science: Materials in Medicine, 21*, 123–130, doi:10.1007/s10856-009-3856-4
33. Einhorn TA. (1998): The cell and molecular biology of fracture healing. *Clinical Orthopaedics and Related Research®*, 355, S7-S21., doi: 10.1097/00003086-199810001-00003.
34. Uzun Kart E. (2021): Evaluation of sulphation baking and autogenous leaching behaviour of Turkish metallurgical slag flotation tailings. *Physicochemical Problems of Mineral Processing. 57*(4),107-116. doi:10.37190/ppmp/138839
35. Wirsching F. (2012): Calcium sulphate. *Ullmann's encyclopedia of industrial chemistry*, 6, 519–550. Doi:10.1002/14356007.a04_555
36. Sony S., Babu S. S., Nishad K. V., Varma H.,Komath M. (2015): Development of an injectable bioactive bone filler cement with hydrogen orthophosphate incorporated calcium sulphate. *Journal of Materials Science Materials in Medicine, 26*, 31–44.doi: 10.1007/s10856-014-5355-5
37. Kuo S.T., Wu H.W., Tuan W.H., Tsai Y.Y., Wang S.F., ve Sakka Y. (2012): Porous calcium sulphate ceramics with tunable degradation rate. *Journal of Materials Science: Materials in Medicine, 23*, 2437–2443. doi: 10.1007/s10856-012-4704-5
38. Rice R. W. (2005): Use of normalized porosity in models for the porosity dependence of mechanical properties. *Journal of Materials Science, 40*, 983–989. doi: 10.1007/s10853-005-6517-0
39. Orsini G., Ricci J., Scarano A., Pecora G., Petrone G., Iezzi G., Piattelli A. (2004): Bone-defect healing with calcium-sulphate particles and cement: an experimental study in rabbit. *Journal of biomedical materials research. Part B, Applied biomaterials, 68,* 199–208. doi: 10.1002/jbm.b.20012
40. Yan Z., Wang Z., Liu H., Tu Y., Yang W., Zeng H., Qiu J. (2015): Decomposition and solid reactions of calcium sulphate doped with SiO_2, Fe_2O_3 and Al_2O_3. *Journal of Analytical and Applied Pyrolysis, 113*, 491–498. doi:10.1016/j.jaap.2015.03.019.